

Original Article

# TiO<sub>2</sub> Particles Influence on the Wear Conduct of an Aluminium AA6061/Red Mud Hybrid Composite

Niranjan Hugar<sup>1</sup>, Venkata Narayana B<sup>2</sup>, Sunil Waddar<sup>3</sup>, Manjunath K<sup>4</sup>, Mohan Kumar K<sup>5</sup>, Santosh N<sup>6</sup>

<sup>1</sup>Research Scholar, Visvesvaraya Technological University-JnanaSangama, Belgaum, Karnataka, India.

<sup>1,2,4</sup>Department of Mechanical Engineering, SEA College of Engineering and Technology, Bengaluru, Karnataka, India.

<sup>3</sup>Department of Mechanical Engineering, JSPM University Pune, Maharashtra, India.

<sup>5,6</sup>Department of Mechanical Engineering, MVJ College of Engineering, Bengaluru, Karnataka, India.

Received Date: 30 November 2023

Revised Date: 29 December 2023

Accepted Date: 21 January 2024

**Abstract:** The current study was carried out with the new goal of developing and characterising high-performance hybrid Aluminium AA 6061/Red Mud composites with varied wt.% TiO<sub>2</sub> (0, 2, and 4% wt.%) for tribological applications. In this regard, ultrasonic-assisted stir casting is used to create composites of various compositions and machine them to ASTM G99-95a standards. The pin-on-disc wear test is performed on a Ducom TR-12 tribometer in accordance with the L27 Orthogonal Array (OA) for varying load parameters of 10 N, 20 N, and 30 N, sliding distances of 500 m, 1500 m, and 2500 m, and disc rotation speeds of 200 RPM, 400 RPM, and 600 RPM, while the hardness test is performed on a Brinell Hardness tester. The results show that the Specific Wear Rate (SWR) and Coefficient of Friction (COF) decrease as the wt.% of TiO<sub>2</sub> increases, although the hardness values rise for the same wt.% of reinforcements. Response Surface Methodology is used to validate the results further (RSM). The hall patch strengthening process is mostly responsible for the increase in hardness and wear resistance.

**Keywords:** Wear, Hardness, Aluminium AA 6061, Red Mud, TiO<sub>2</sub>.

## 1. INTRODUCTION

The importance of aluminium composites in engineering applications has grown as a result of the numerous benefits they provide. However, one of the drawbacks that must be overcome is the distribution of reinforcements in the aluminium matrix. The use of inoculants in this regard can result in casting homogeneity [1], and the requirement of such composites has resulted in advancements in various processing techniques to attain these enormous possibilities [2,3]. Stir casting is a prominent process approach for composite fabrication due to the advantages that the technology has over other manufacturing processes; this strategy produces composites with uniform qualities. In comparison to traditional process approaches, stir casting procedures have allowed for the development of a vast array of composites. Ceramic reinforcements dispersed across a metallic network will often provide the optimal combination of mechanical qualities [4]. However, it results in embrittlement. Furthermore, the great bulk of MMC research is focused on reinforcing ceramic particles in Al-based composites to improve mechanical properties by the fusion of ceramic particulates into the metallic lattice. Nonetheless, the usage of carbides, borides, and metal oxides inside the Al metallic grid is accomplished via solid bonding between the carbides and framework at temperatures exceeding 720° C, in the presence of degassers that improve their solidity. Significant research on inoculants promoting uniform dissemination is required to address these deficiencies. TiO<sub>2</sub> offers exceptional lubricity and bonding properties at higher temperatures when compared to other inoculants. The TiO<sub>2</sub> inoculants, in particular, have a stronger impact on the uniform distribution of red mud reinforcements in the matrix phase. Because of its properties, the usage of TiO<sub>2</sub> as inoculants is critical. Until yet, the potential of TiO<sub>2</sub> for better nanophase is still in its early stages, necessitating additional research.

The red mud, on the contrary hand, is a byproduct of the Bayers process, and its dumping poses a major environmental threat that must be dealt with urgency. The incorporation of this red mud reinforcement into the matrix will give a long-term solution for dealing with this byproduct. The uniform distribution of red dirt in the matrix, on the other hand, is a serious challenge that must be addressed [5]. Several researchers have attempted, but failed, to disperse red mud uniformly using SiC coated mild steel stirrers with bow shaped cutting edges in stir casting furnaces [7-9]. As a result, inoculants are required to enhance the process of reinforcement distribution in the matrix. In this respect, Santhosh N et al. discovered that additives in the form of fly ash can be suitably spread inside the Al grid, as well as the use of hetero-conglomerates and fly ash inoculants can improve the bonding between the framework and the fortifications [10]. This advancement has inspired the cautious use of inoculants, which strengthen the bonds between the constituents [11]. The inclusion of 2.5 wt.% fly debris in the Al grid composite enhanced bonding strength by 35% in comparison to the Al base metal, as well as a 15.6% reduction in composite wear rate [12]. Furthermore, the inoculants have a considerable impact on



the hardness and impact strength parameters of the composites [13-15]. F Rana et al. [16] conducted extensive research on the combination and representation of Al network composites and demonstrated that ceramic reinforcements have a substantial impact on composite performance due to embrittlement. K S Al Rubaie et al. [17] published their findings on the wear characteristics of Al lattice composites, describing how the introduction of carbide reinforcements increases the composites' resistance to wear due to the creation of Al-C bonds and orowan strengthening at the nuclear level. Furthermore, it is critical to statistically validate the results of the experiments, which Y Sahin et al. [18] have done by comparing the factual investigations using Taguchi Procedures and highlighting that the optimization of the process parameters significantly affects the wear in the composite specimens. Thus, the use of inoculants and the adjustment of process parameters in tribological studies will reduce wear, and the evaluation of ideal measures of fortifications will result in higher bonding in the composite. The adjustment of process parameters for experimental trials significantly improves the wear conductivity of the composites [19-22]. studies to improve composite tribological performance [23-25]. Various scientists have emphasised the need of using appropriate inoculants and conducting optimization studies for improved tribological performance of composites [23-25]. As a result, the purpose of this research is to investigate the wear behaviour of AA 6061/TiO<sub>2</sub>/Red Mud composites, collect data for statistical validation of the wear experiments using Response Surface Method-based optimization techniques, and investigate the influence of TiO<sub>2</sub> inoculants on the tribological properties of the composites.

**II. MATERIALS AND METHODS**

**A. Materials:**

Aluminium AA 6061 matrix is utilised in this work because it is used for automotive applications and has superior formability, weldability, better strength, corrosion resistance, and can be easily forged into needed shape and size. The principal alloying constituents of Aluminium AA 6061 are Si and Mg, and it may easily bond with the reinforcements. The composition of the Aluminium AA 6061 matrix alloy determined from the EDS is shown in table 1. The existence of Si and Mg as the principal alloying elements is determined by EDS analysis, as is the case with the compositional criteria provided by the Aluminium Association for 6061 grade alloy. The parameters of the AA 6061 alloy as provided by the supplier data sheet [PMC Metal Corporation, Bengaluru, Karnataka] are listed in table 2.

**Table 1: Elemental Composition Obtained from the EDS Analysis**

Element	Mg	Al	Si	Cr	Mn	Fe	Cu	Zn
Weight %	1.38	93.41	1.29	0.64	0.42	1.64	0.72	0.52
Atomic %	1.56	95.3	1.26	0.34	0.21	0.81	0.31	0.22

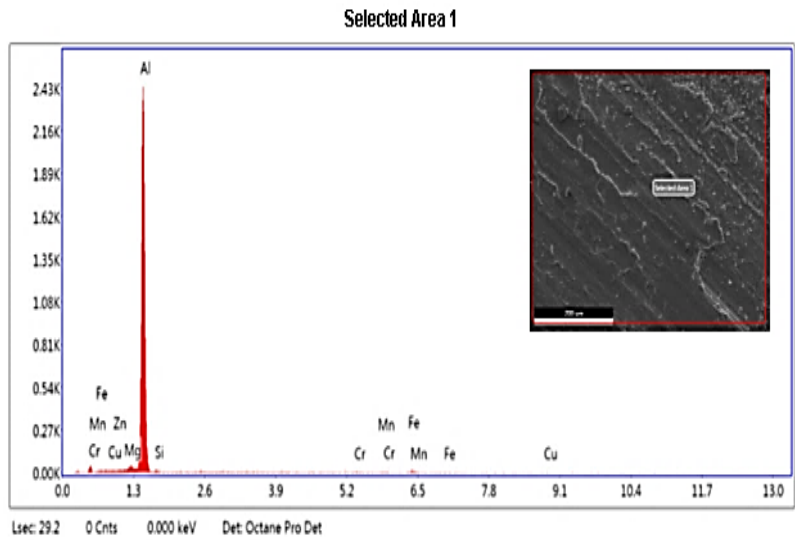


**Figure 1: EDS Spectrum of as Cast Aluminium AA 6061 Alloy**

**Table 2: Property Table Provided by the Supplier Data Sheet**

Property	Value
Density	2.7 g/cm <sup>3</sup>
Brinell Hardness	95 BHN
Ultimate Tensile Strength	310 MPa
Yield Strength	276 MPa
Youngs modulus	68.9GPa

Coefficient of Thermal Expansion	23.6 $\mu\text{m}/\text{m}^\circ\text{C}$
Thermal Conductivity	167 W/mK

The red mud is obtained from the National Aluminium Company (NALCO) in Gujarat, and SEM characterization is performed to validate the size and shape of the red mud particles, as well as EDS to confirm the composition of compounds found in redmud. Figure 2a depicts a SEM image of the red mud particles, whereas Figure 3 depicts an EDS analysis of the red mud sample.

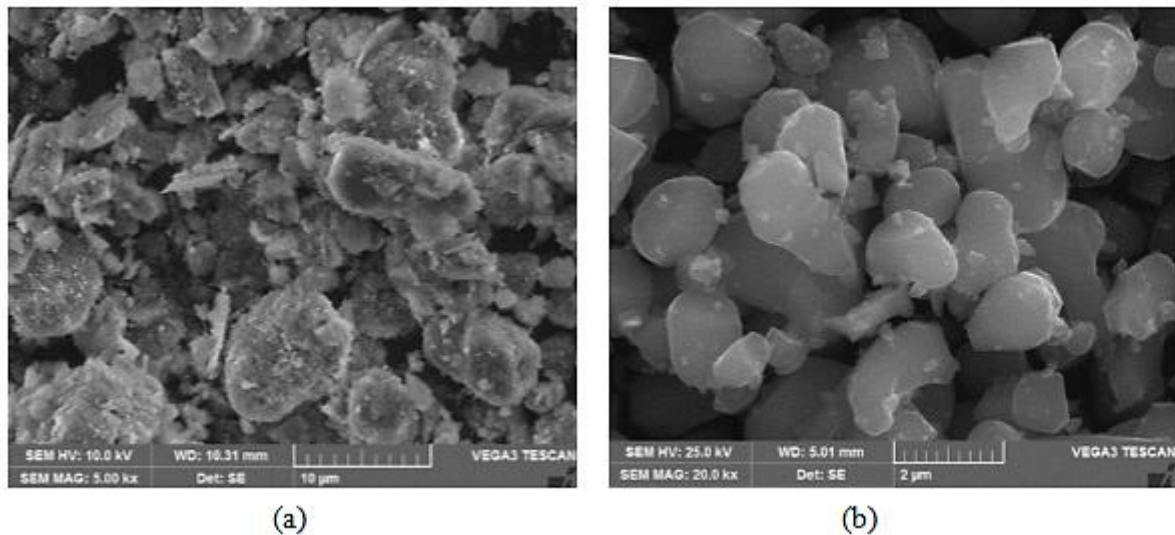


**Figure 2: (a). SEM Image of Red Mud Particles and (b). SEM Image of  $\text{TiO}_2$  particles**

The EDS spectrum of the red mud particles in figure 3 clearly reveals the presence of the oxides of Al, Fe, and Si, with traces of Ti, which comprise the redmud's composition. When combined in appropriate quantities with the AA 6061 matrix, the ceramic compounds in the red mud tend to offer better wear resistance.

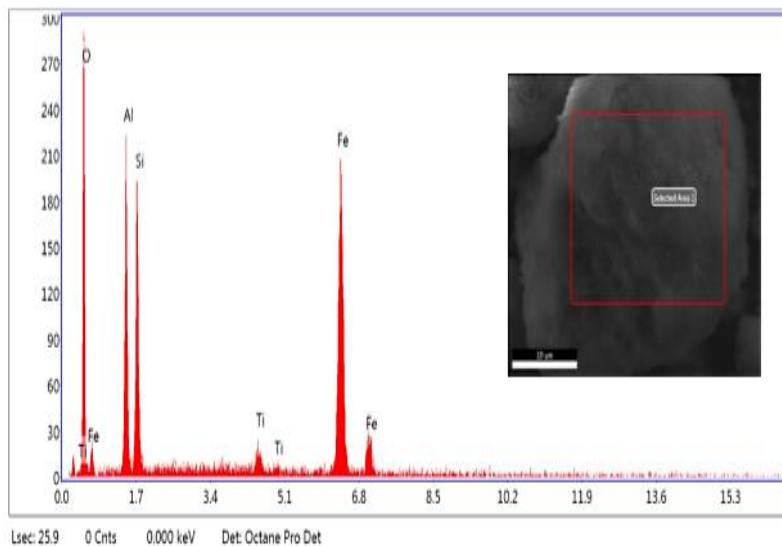


**Figure 3: EDS Spectrum of Red Mud Particles**

The  $\text{TiO}_2$  is obtained from NIMCO Metals in Bengaluru, and SEM characterisation is performed to confirm the size and shape of the particles. Figure 2b is a SEM picture of  $\text{TiO}_2$  particles.  $\text{TiO}_2$  particles with tetragonal forms are found to be 2 - 10 m in size.

**B. Casting and Specimen Preparation:**

The weighted proportions of the aluminium AA 6061 alloy pieces are fed into the stir casting furnace's crucible and melted at a temperature of 690 oC in an inert gas environment to prevent atmospheric oxygen from becoming trapped in the molten metal. Hexachloroethane degassing tablets are dropped into the molten metal to remove the oxides and associated impurities that cause the slag to be scraped from the surface of the molten metal. After the slag has been removed

from the molten metal, the weighed proportions of preheated  $\text{TiO}_2$  and Red mud reinforcements are added, along with 0.5 g of magnesium wrapped in aluminium foil. The mixture is then heated to a temperature of  $720^\circ\text{C}$  and stirred continuously for two periods of 10 minutes each. The addition of coverall flux is then added for one more cycle of degassing, and the slag is then scraped off the molten metal's surface. While the composition of the  $\text{TiO}_2$  inoculants varies from 2 to 6 weight percent, the weight percent of red mud is kept constant at 2 weight percent. Prior to conducting actual research tests, the composition of the reinforcements is taken into consideration based on an analysis of the existing literature and the initial set of pilot trials. When the flux is added, red mud that has been added in excess of 2 weight percent will aggregate and eventually release as slag. This is the key obstacle that is restricting the composition of red mud in the matrix. Additionally, Santhosh N et al. [26] indicated that an increase in reinforcements above 10 weight percent will cause the reinforcements to aggregate in the matrix, which will lead to an uneven distribution of particulates and the creation of voids in certain localised areas. The matrix and reinforcements in the composites created in this work are described in table 3 along with their composition.

**Table 3: Composition of Composite Specimens**

Composition	Wt % of Red Mud	Wt % of $\text{TiO}_2$	Wt % of AA 6061
AS CAST	0	0	100
AR2T2	2	2	96
AR2T4	2	4	94

The castings are then cut to the required dimensions for the ASTM G99-95a test specifications. The specimens' length is 30 mm and their diameter is 8 mm. The pin on disc test specimen's schematic is shown in figure 4.

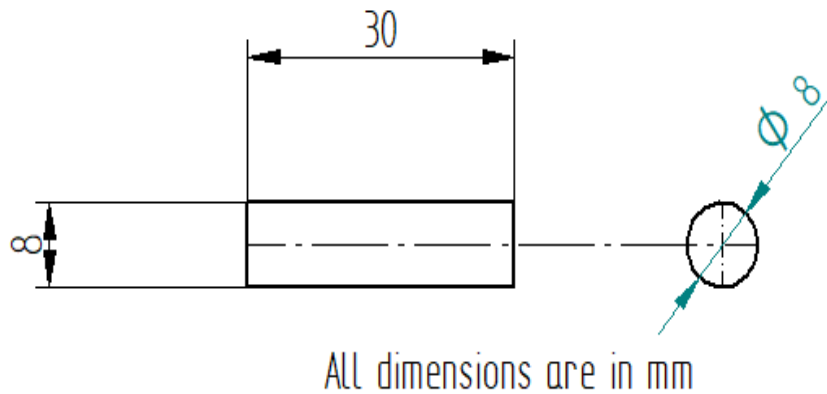


**Figure 4: Sketch of the Pin on the Disc Specimen**

### C. Experimental

The experiments are carried out to determine the wear properties and hardness of the composite specimens. On a Brinell Hardness Tester made by Fine Instruments, the hardness tests are conducted. In a Brinell hardness test, a 5 mm ball indenter is employed with a load application of 250 kgf and a dwell time of 30 seconds for each specimen at various points. In accordance with ASTM E10-18, numerous experiments are carried out to identify the specimens, and the outcomes are averaged and tabulated.

On a tribometer by Ducom, model ED-201, wear tests are carried out in line with ASTM G99-95a test requirements. The initial set of pilot trials and the current literature review are used to help choose the test parameters for the wear characterisation. The L9 orthogonal array (OA) is used to design the experiments for carrying out the wear tests. The loads considered for the experimental trials range from 10 N to 30 N with an interval of 10 N between each trial, sliding distances from 500 to 2500 m with an interval of 1000 m between trials, and disc rotation speeds from 200 to 600 rpm with an interval of 200 rpm between trials. The investigations are carried out with the pin on disc specimens clamped against a rotating EN 32 grade steel disc. For each of the trials, the eqn 1's Friction Force (FF) and Coefficient of Friction (COF) are recorded. Additionally, the volume loss resulting from wear is calculated by deducting the specimen's post-wear volume from its initial volume. The specific wear rate (SWR) is then determined using the eqn 2 and this magnitude of volume loss. Following experimental trials, optimization studies using the Response Surface Methodology (RSM) are conducted on the COF and SWR values to improve the process parameters. To investigate how process parameters affect the rate of wear for each composite specimen, the statistical results and experimental data are further evaluated, and error predictions are made. After that, Scanning Electron Microscopy is used to analyse the surface morphology of the worn surfaces, and the wear debris is thoroughly investigated in order to comprehend the wear mechanism.

$$\text{Coefficient of Friction [COF}(\mu)] = \frac{F}{N} \quad (1)$$

Where,  $F$  is the Frictional Force, and  $N$  is the Normal Force.

$$\text{Specific Wear Rate (SWR)} = \frac{\text{Wear Volume Loss in mm}^3}{(\text{Sliding Distance in m} \times \text{Applied Load in N})} \quad (2)$$

Where, wear volume loss is given by  $V_{Loss} = \frac{\pi \times d^2}{4} \times \text{Wear loss in mm}$

#### D. Response Surface Methodology (RSM) studies

RSM investigations are conducted in order to improve and statistically verify the results of experiments. By taking into account the three process parameters of the wear experiments—the load (X) in N, the sliding distance (Y) in m, and the disc rotation (Z) in RPM—the COF and SWR are validated. These parameters are then modelled for the response optimization based on the three factor approach. According to the process parameters, the response is given by equation 3.

$$\lambda = f(X, Y, Z) \quad (3)$$

Where,  $\lambda$  is the response viz., COF and SWR modeled as a function of the factors X, Y and Z.

Additionally, the three factors and three levels for each factor as shown in table 4 are taken into account while modelling the regression equations. By taking into account the Coefficient of Correlation (R<sub>2</sub>), adjusted R<sub>2</sub> and anticipated R<sub>2</sub> values, the experimental results are statistically confirmed. The produced surface and contour plots show the variation in responses across the various factorial levels.

**Table 4: Factors and their Levels used for the Wear**

Level	Load(X) in N	Sliding Distance [Y] in m	Disk Rotation [Z] in RPM
1	10	500	200
2	20	1500	400
3	30	2500	600

The L<sub>9</sub> orthogonal array-based experimental results are statistically confirmed using the RSM. The key factors are determined from the statistical comparisons, and optimization studies are completed.

Following sample fabrication, a SEM analysis is carried out to understand the uniform mixing of the materials. Additionally, the microstructural analysis provides details regarding the wear mechanism, the surface properties of the worn surfaces, and the shape of the wear track [27–32]. A foundation for assessing the contact mechanics during the adhesive wear process is provided by the wear track analysis [33–36].

### III. RESULTS

#### A. Scanning Electron Microscopy (SEM) and XRD Studies

A VEGA 3 TESCAN LMU machine with a scanning voltage of 25 kV, a resolution range of 3.1 nm to 15.5 nm, a magnification range of 4.5 X to 1,000,000 X, and a five axis control is used to perform scanning electron microscopy at the BMS College of Engineering.

Following sample production, a SEM analysis is carried out to understand the uniform mixing of the reinforcements in the matrix. The SEM images make it obvious that the TiO<sub>2</sub> and Redmud are uniformly distributed. It asserts that the stir casting process parameters led to improved dispersion being attained. Also worth mentioning is the strong adhesion between the components, which is evident in the SEM images. The TiO<sub>2</sub> and Redmud particle aggregation is not visible in the micrographs [figure 5(a)]. Although there are more particles visible in the SEM micrographs [figures 5(b) and 5(c)] when the weight percent of TiO<sub>2</sub> rises, the number of Redmud particles is constant across all SEM photos.

On a Panalytical Xpert brand XRD machine with a voltage of 35 kV and a current of 50 mA, the X-ray diffraction studies on the composite species of ASCAST (Figure 6a), AR2T2 (Figure 6b), and AR2T4 (Figure 6c) are completed. The XRD is carried out by the diffractometer using Cu-Kα radiation. The approximate observed peaks for the Al6061 alloy alloying elements are shown in Figure 6a at 38.83°, 45.07°, 65.38°, and 78.47°. Peaks are shown at 38.78°, 38.98°, 45.06°, 45.22°, 65.51°, 78.47°, and 78.76° in the specimens of the 2 weight percent redmud and 2 weight percent TiO<sub>2</sub> reinforced composite, indicating the presence of redmud and TiO<sub>2</sub> compounds. Figure 6c depicts the 2 weight percent redmud and 4 weight percent TiO<sub>2</sub> reinforced Al6061 composite. The peaks at 38.84°, 45.03°, 65.39°, 78.46°, and 82.66°, respectively, indicate the presence of Red mud and TiO<sub>2</sub> compounds. Al6061 composites contain redmud and TiO<sub>2</sub>, as shown by the x-ray diffractograms.

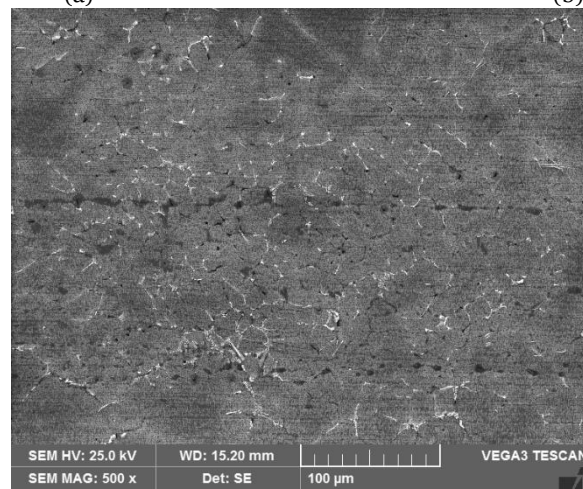
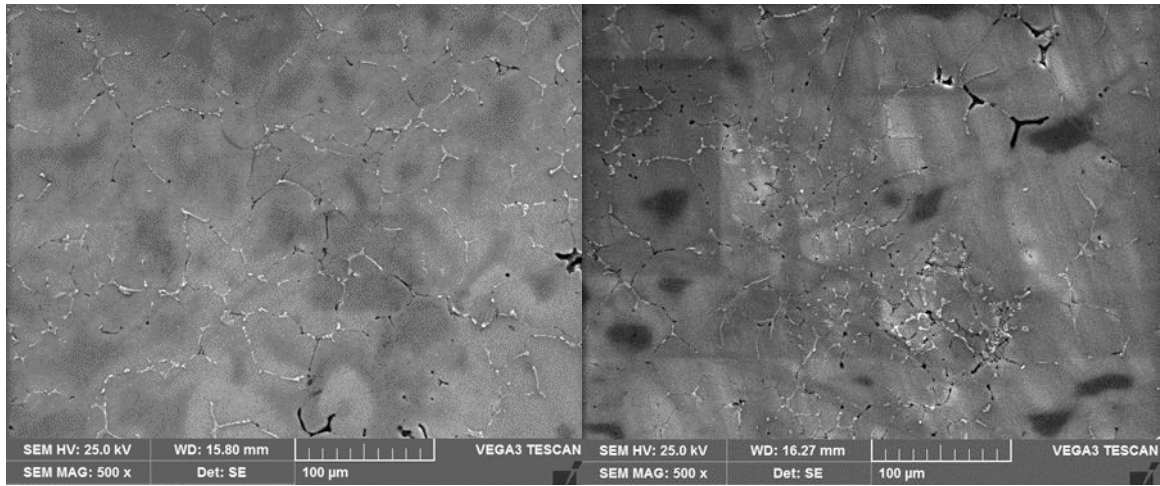
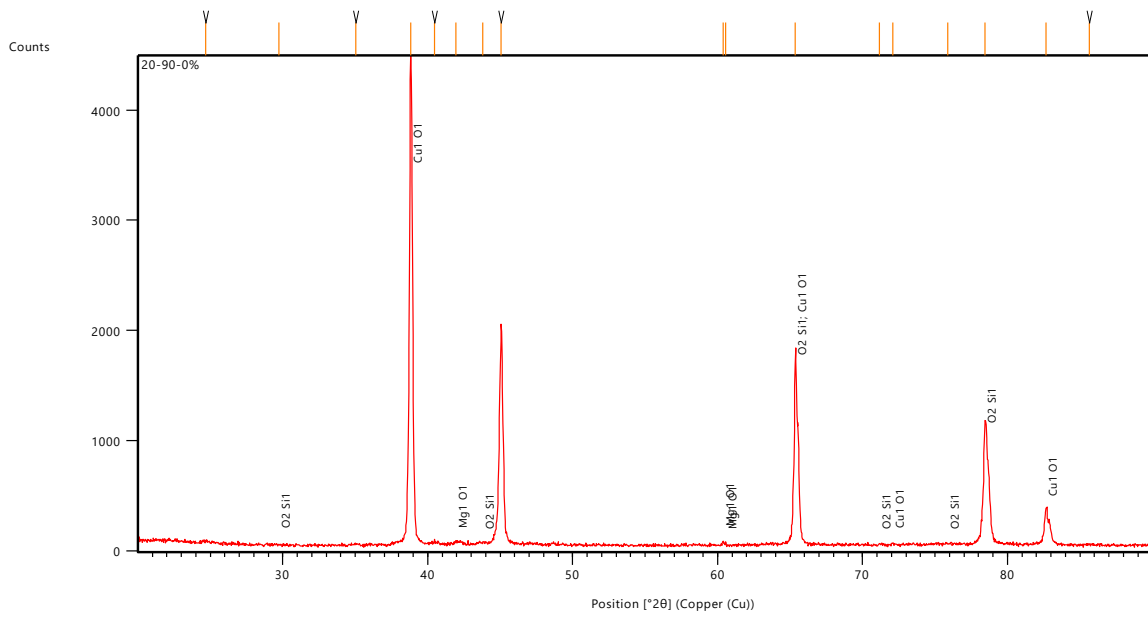


Figure 5: SEM micrographs of specimen before testing. (a) ASCAST (b) AR2T2. (b) AR2T4



(a)



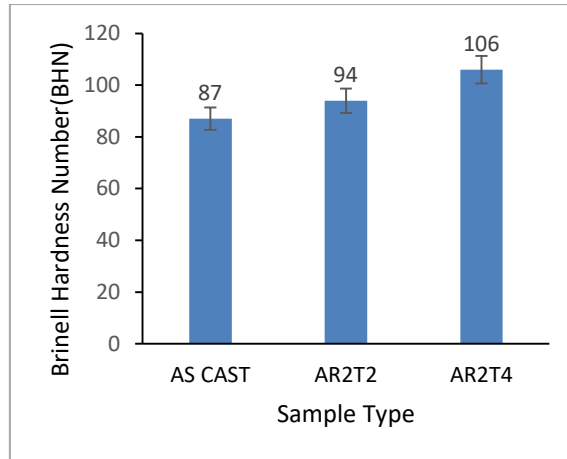


Figure 7: Brinell Hardness of. (a) ASCAST (b) AR2T2. (b) AR2T4

### C. Effect of the different factors on COF and SWR for As Cast Specimen

A Ducom ED-201 tribometer is used to perform the pin on disc wear test in a controlled setting. Using a data collecting equipment connected to the computer, the dataset for friction force is obtained for various factorial levels over a runtime of 600 seconds. The COF and the SWR are then calculated and tabulated for various factorial values. The results of the experiments are validated and employed in statistical modelling with RSM. Table 5 summarises the findings of the studies for As Cast and various composite specimen compositions.

Table 5: Wear results for the as Cast and Composite Specimens

Wt.% of Red Mud	Wt.% of TiO <sub>2</sub>	LOAD (N)	SLIDING DISTANCE (m)	DISK ROTATION (RPM)	SWR (mm <sup>3</sup> /N-m)	COF
0	0	10	500	200	0.00626	0.339
0	0	10	1500	400	0.00562	0.354
0	0	10	2500	600	0.00514	0.366
0	0	20	500	200	0.00568	0.351
0	0	20	1500	400	0.00531	0.363
0	0	20	2500	600	0.00422	0.376
0	0	30	500	200	0.00453	0.362
0	0	30	1500	400	0.00359	0.389
0	0	30	2500	600	0.00275	0.411
2	2	10	500	200	0.00529	0.336
2	2	10	1500	400	0.00456	0.351
2	2	10	2500	600	0.00405	0.359
2	2	20	500	200	0.00461	0.348
2	2	20	1500	400	0.00425	0.354
2	2	20	2500	600	0.00315	0.363
2	2	30	500	200	0.00341	0.351
2	2	30	1500	400	0.00253	0.376
2	2	30	2500	600	0.00169	0.401
2	4	10	500	200	0.00471	0.328
2	4	10	1500	400	0.00411	0.341
2	4	10	2500	600	0.00359	0.354
2	4	20	500	200	0.00416	0.349
2	4	20	1500	400	0.00376	0.357
2	4	20	2500	600	0.00265	0.363
2	4	30	500	200	0.00302	0.344
2	4	30	1500	400	0.00204	0.368
2	4	30	2500	600	0.00128	0.389

#### a) Statistical Validation of SWR for As Cast and Composite Specimens

Utilizing RSM methodologies, the wear findings are statistically validated, and surface and 3D contour plots are produced. The Analysis of Variance (ANOVA) is then used to separate the observed data and learn enough about how the

dependent and independent variables in the wear test relate to one another. The interaction plot is shown in figure 8, the prediction plots for SWR are shown in figure 9(a), and the 3D surface plot for SWR is shown in figure 9(b).

A plot for the curve fitting the predicted vs. actual data is also provided by the RSM in figure 9(a), together with the ANOVA table (Table 6), fit data (Table 7), and curve fitting data. While equation 4 provides the regression equation for the SWR values acquired from the Minitab Software using the RSM model.

Table 6: ANOVA table for SWR for As Cast and Composite Specimens

Source	DF	Adj SS	Adj MS	F-Value	P-Value
Model	11	0.000041	0.000004	216.08	0
Linear	4	0.00003	0.000007	433.06	0
Wt.% of Red Mud	1	0.000001	0.000001	30.62	0
Wt.% of TiO2	1	0.000001	0.000001	57.37	0
LOAD (N)	1	0.000012	0.000012	721.59	0
SLIDING DISTANCE (m)	1	0.000006	0.000006	368.28	0
Square	2	0.000001	0.000001	30.46	0
LOAD (N)*LOAD (N)	1	0.000001	0.000001	58.96	0
SLIDING DISTANCE (m)*SLIDING DISTANCE (m)	1	0	0	1.96	0.182
2-Way Interaction	5	0	0	3.04	0.043
Wt.% of Red Mud*LOAD (N)	1	0	0	0.16	0.69
Wt.% of Red Mud*SLIDING DISTANCE (m)	1	0	0	0.02	0.891
Wt.% of TiO2*LOAD (N)	1	0	0	0.19	0.666
Wt.% of TiO2*SLIDING DISTANCE (m)	1	0	0	0.01	0.914
LOAD (N)*SLIDING DISTANCE (m)	1	0	0	14.97	0.002
Error	15	0	0		
Total	26	0.000041			

Table 7: Model Summary for SWR

S	R-sq	R-sq (adj)	R-sq (pred)
0.000131	99.37%	98.91%	98.37%

$$\begin{aligned}
 SWR \left( Cu. \frac{mm}{N} - m \right) = & 0.005998 - 0.000230 * Wt. \% \text{ of Red Mud} - 0.000274 * Wt. \% \text{ of TiO2} + 0.000084 * \\
 & LOAD (N) - 0.0000001 * SLIDING DISTANCE (m) - 0.000004 * LOAD (N) * LOAD (N) - 0.0000001 * \\
 & SLIDING DISTANCE (m) * SLIDING DISTANCE (m) - 0.000003 * Wt. \% \text{ of Red Mud} * LOAD (N) - 0.0000001 * \\
 & Wt. \% \text{ of Red Mud} * SLIDING DISTANCE (m) + 0.000002 * Wt. \% \text{ of TiO2} * LOAD (N) + 0.0000001 * \\
 & Wt. \% \text{ of TiO2} * SLIDING DISTANCE (m) - 0.0000001 * LOAD (N) * SLIDING DISTANCE (m)
 \end{aligned} \tag{4}$$

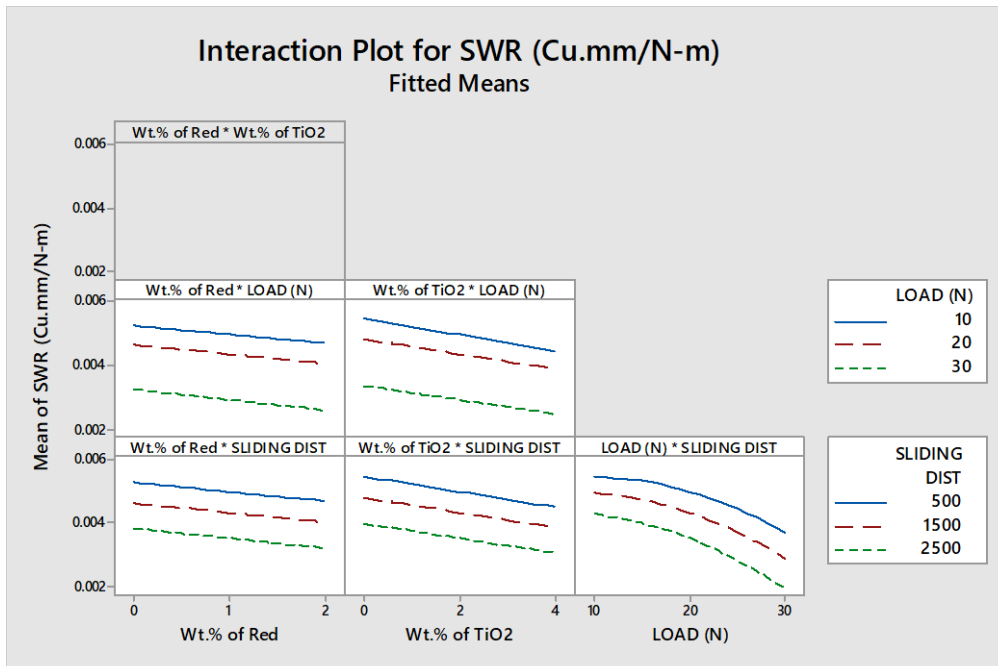


Figure 8: Interaction Plot for SWR

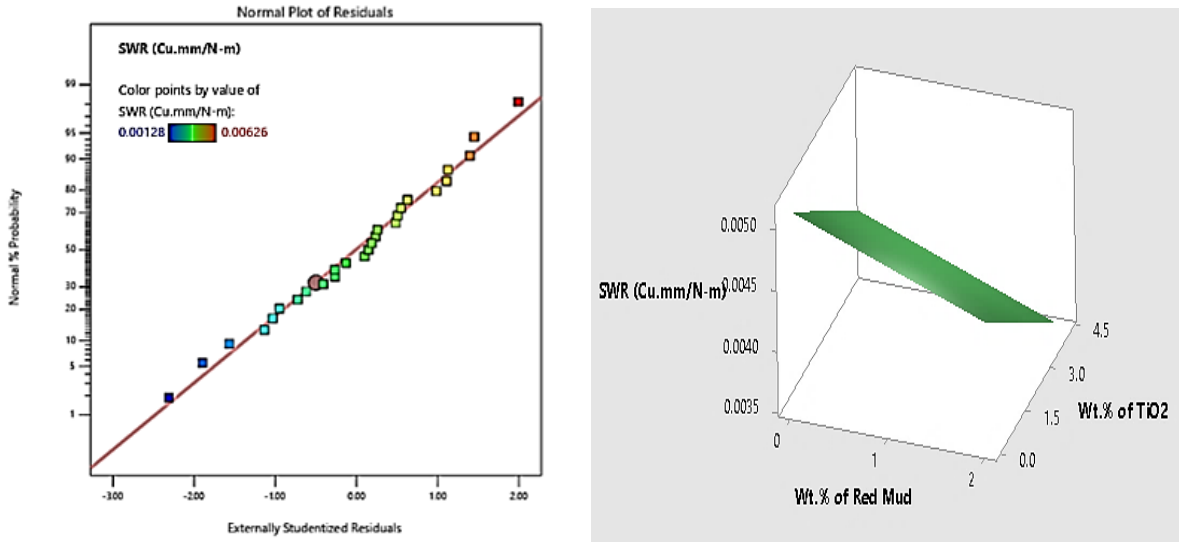


Figure 9. (a) Prediction Plot and (b) 3D surface plot for SWR

The values of  $R^2$  and Adjusted  $R^2$  are 99.37% and 98.91%, respectively. This suggests that the correlation coefficient is close to 1 and that the projected values and experimental values fit linearly, with a reasonably small number of outliers.

The P values are less than 0.05 for the linear model, which includes the parameters of Wt.% of Red Mud, Wt.% of TiO<sub>2</sub>, load, and sliding distance in the ANOVA table to indicate the influence of individual components.

However, all interactions aside from the interaction between load and sliding distance have P values for two-way interactions that are more than 0.05. The design space for linear regression and one-way interactions can now be explored using this approach.

*b) Statistical Validation of COF for As cast specimen and composite specimens*

For the Coefficient of Friction (COF) data, statistical validation is done for As cast and composite specimens. Table 8 provides the COF ANOVA table for As Cast and Composite Specimens, while Table 9 provides a model summary for the fit data for COF. Figure 10 displays the interaction plot, Figure 11 (a) displays the anticipated vs. actual data plot, and Figure 11 (b) displays the 3D surface plots for COF.

The regression correlation also provides equation 5, which is the regression equation from the RSM model for the COF data. While the wear loss increases with an increase in COF, the SWR decreases because the volumetric wear loss is considerably less than the load and sliding distance increases that follow.

Table 8: ANOVA table for COF for As Cast and Composite Specimens

Source	DF	Adj SS	Adj MS	F-Value	P-Value
Model	11	0.009367	0.000852	25.34	0.0001
Linear	4	0.006399	0.0016	47.61	0.0001
Wt.% of Red Mud	1	0.000013	0.000013	0.37	0.551
Wt.% of TiO <sub>2</sub>	1	0.000118	0.000118	3.5	0.081
LOAD (N)	1	0.00273	0.00273	81.24	0.0001
SLIDING DISTANCE (m)	1	0.002883	0.002883	85.79	0.0001
Square	2	0.000098	0.000049	1.46	0.264
LOAD (N)*LOAD (N)	1	0.000093	0.000093	2.78	0.116
SLIDING DISTANCE (m)*SLIDING DISTANCE (m)	1	0.000005	0.000005	0.14	0.712
2-Way Interaction	5	0.00047	0.000094	2.79	0.056
Wt.% of Red Mud*LOAD (N)	1	0.000008	0.000008	0.24	0.632
Wt.% of Red Mud*SLIDING DISTANCE (m)	1	0.000003	0.000003	0.08	0.778
Wt.% of TiO <sub>2</sub> *LOAD (N)	1	0.000001	0.000001	0.04	0.845
Wt.% of TiO <sub>2</sub> *SLIDING DISTANCE (m)	1	0.000001	0.000001	0.02	0.883
LOAD (N)*SLIDING DISTANCE (m)	1	0.000385	0.000385	11.47	0.004
Error	15	0.000504	0.000034		
Total	26	0.009871			

**Table 9: Model Summary for COF**

S	R-sq	R-sq(adj)	R-sq(pred)
0.005797	94.89%	91.15%	83.15%

COF =

$$0.3370 + 0.00264 * \text{Wt. \% of Red Mud} - 0.00151 * \text{Wt. \% of TiO}_2 - 0.00071 * \text{LOAD (N)} + 0.000008 * \text{SLIDING DISTANCE (m)} + 0.000039 * \text{LOAD (N)} * \text{LOAD (N)} - 0.0000001 * \text{SLIDING DISTANCE (m)} * \text{SLIDING DISTANCE (m)} - 0.000142 * \text{Wt. \% of Red Mud} * \text{LOAD (N)} - 0.000001 * \text{Wt. \% of Red Mud} * \text{SLIDING DISTANCE (m)} - 0.000033 * \text{Wt. \% of TiO}_2 * \text{LOAD (N)} - 0.0000001 * \text{Wt. \% of TiO}_2 * \text{SLIDING DISTANCE (m)} + 0.000001 * \text{LOAD (N)} * \text{SLIDING DISTANCE (m)} \quad (5)$$

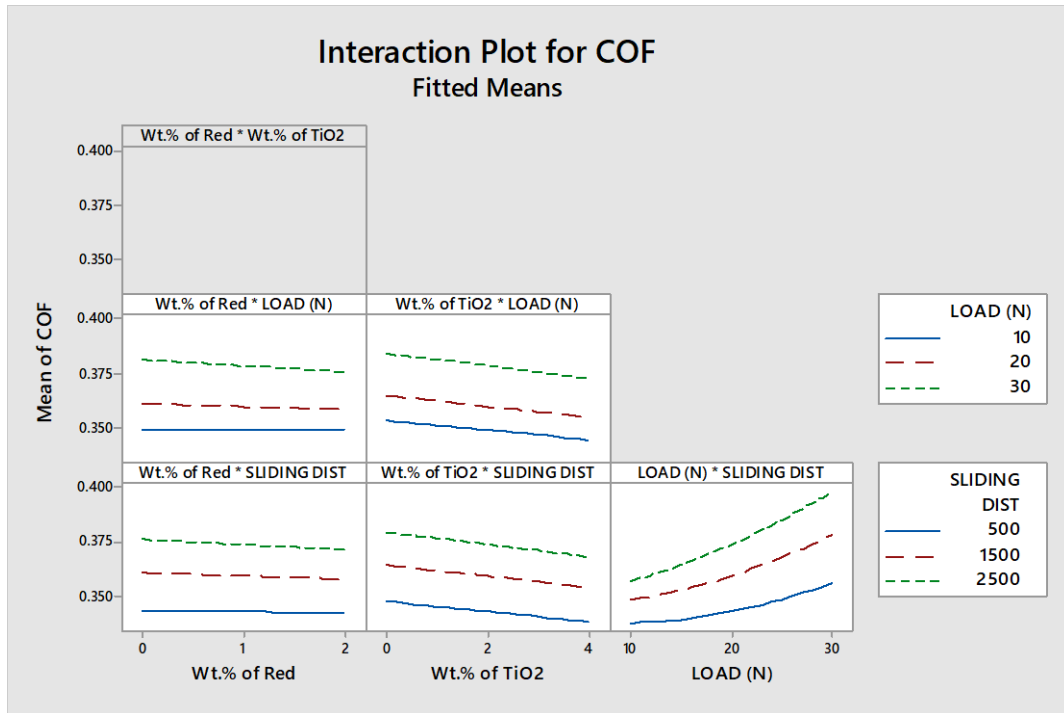


**Figure 10: Interaction Plot for COF**

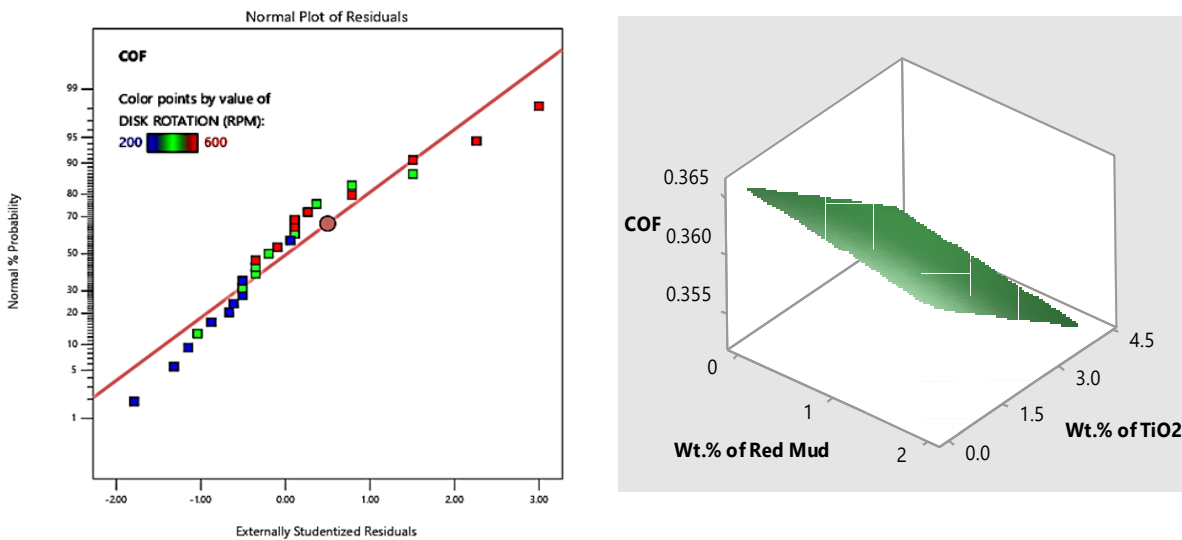


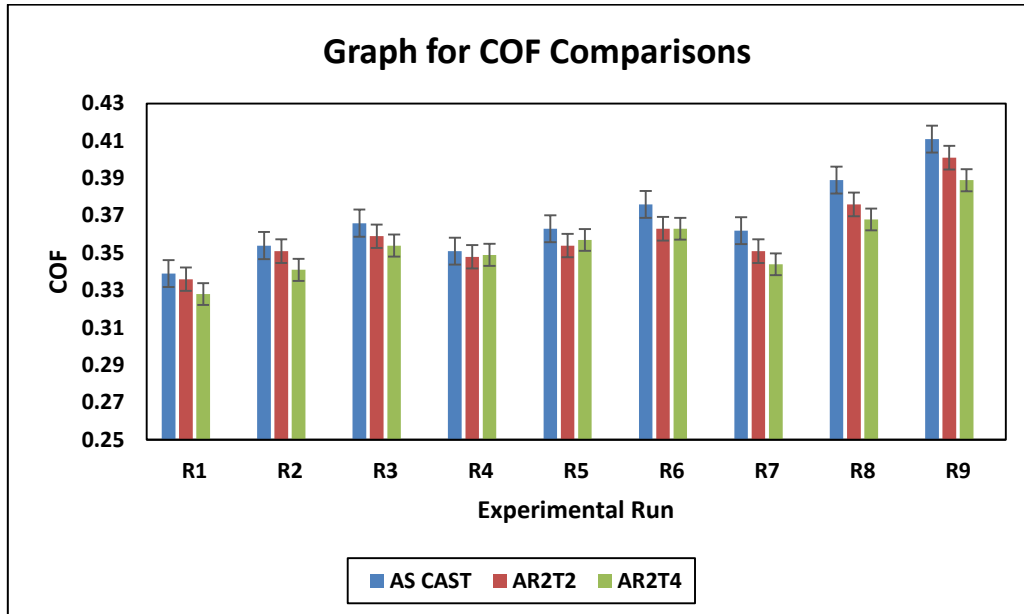
**Figure 11. (a) Prediction plot and (b) 3D surface plot for COF**

The adjusted  $R^2$  value is 91.15%, while the  $R^2$  value is 94.89%. The projected values and experimental values fit linearly, indicating that the correlation coefficient is close to 1. With some negligible outliers, the expected  $R^2$  is 83.15, though. In comparison to the weight and sliding distance, the P values for the red mud and TiO<sub>2</sub> are more than 0.05. As a

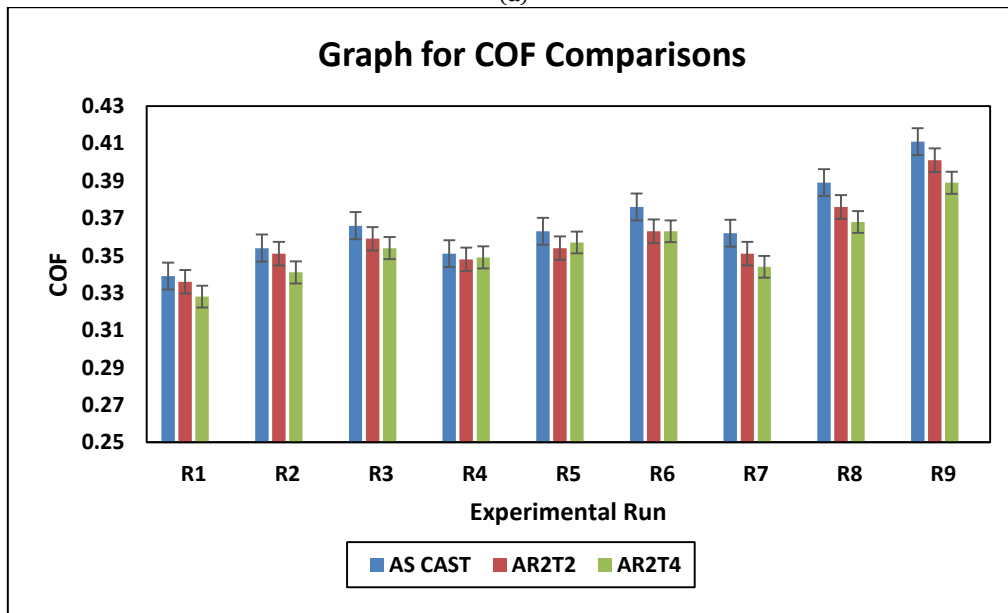
result, while decreasing the wear of the composite materials, red dirt and TiO<sub>2</sub> are not having a substantial impact on friction. Therefore, the model supports the claim that the chosen reinforcement lowers friction while raising hardness and wear resistance.

**D. Comparisons for SWR and COF for different composite specimens**

Figures 12(a) and 12(b) compare the SWR and COF values for various composite specimens, and clearly show that the SWR decreases when red mud and TiO<sub>2</sub> reinforcements are incorporated into the matrix. This is owing to the ceramic compounds, specifically the oxides of Ti and the oxides of Al and Fe in the redmud, which produce embrittlement and a subsequent rise in hardness. The friction between the surfaces is unaffected by the increased TiO<sub>2</sub> content, though. Red mud and TiO<sub>2</sub> content increases have further accelerated agglomeration while also making surfaces more brittle and abrasive. The focus of the current effort is now limited to 4 weight percent TiO<sub>2</sub> and 2 weight percent redmud.



(a)



(b)

**Figure 12: Graph for (a)SWR Comparisons and (b) COF Comparisons**

It is clear from the experimental findings and statistical analysis that 2 weight percent red mud and 4 weight percent TiO<sub>2</sub> are the ideal reinforcing weight percentages for enhancing the wear properties in composites. Additionally, this is determined from the COF and SWR comparison graphs.

### E. Scanning Electron Microscopy of Wear Track

Figure 13 shows the SEM of the wear track of the composite specimens for the weight percentage of the reinforcements. The SEM photos clearly show that the as-cast specimen has more ridges and valleys, but the number of ridges, valleys, and wear tracks decreases as the weight percentage of the reinforcements increases. The creation of friction coatings, which resist indentation and surface abrasion, is thought to have reduced the amount of wear tracks.

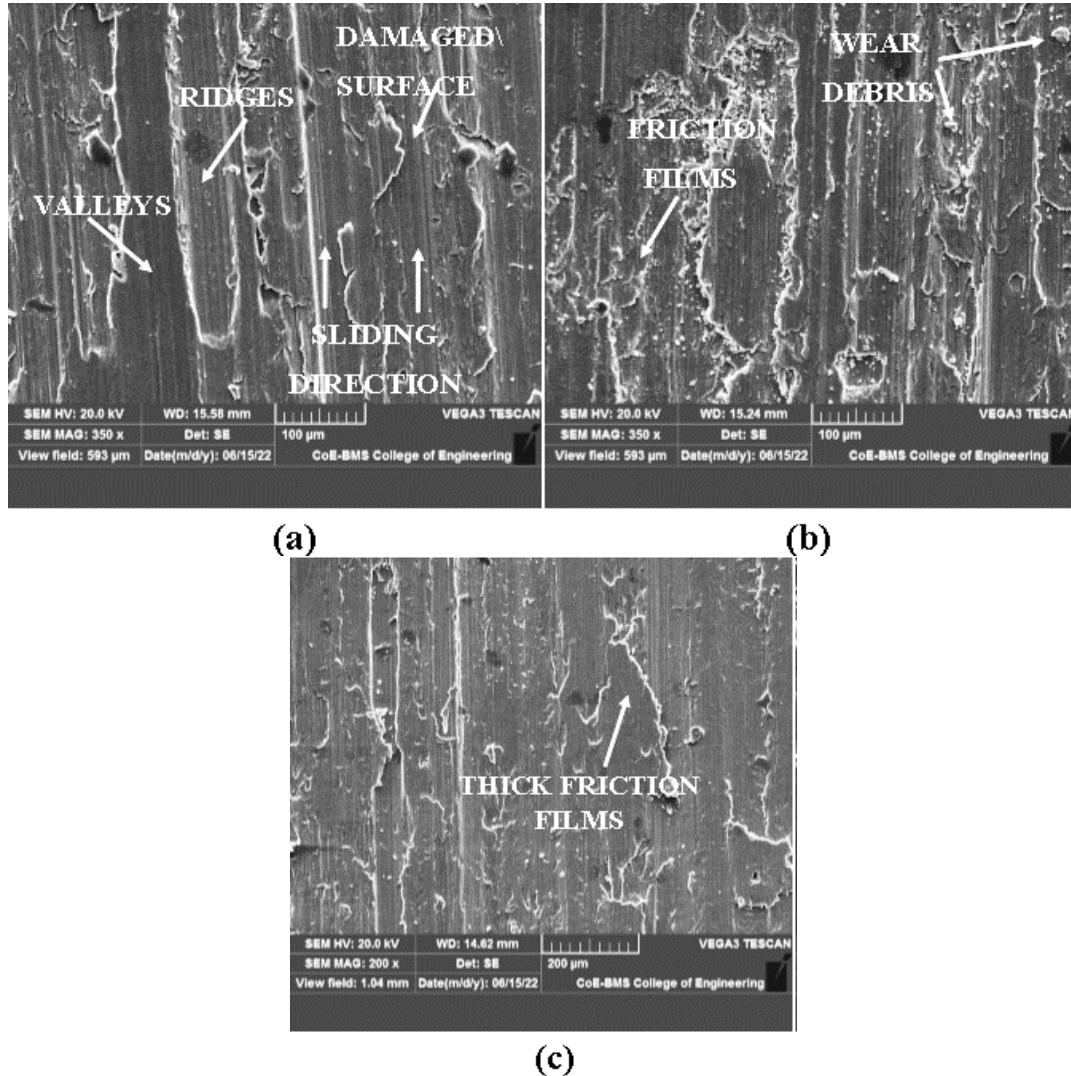


**Figure 13: SEM images of the Worn Surface of (a) as Cast (b) AR2T2 (c) AR2T4 Composite Specimens**

Figure 13 (a) displays a SEM image of the as-cast specimen with cracked surfaces and obvious ridges and valleys. While the SEM picture of the AR2T2 specimen with worn debris and the thin layers of friction films that start to form when reinforcements are added is shown in figure 13(b), The AR2T4 specimen's SEM picture is shown in Figure 13(c), and it has thick friction coatings that prevent specimen wear and tear.

### IV. CONCLUSION

TiO<sub>2</sub> and red mud composites have been effectively manufactured using the stir casting technique, with homogeneous distribution of reinforcements for the best weight percentage. The red dirt and TiO<sub>2</sub> particles have been successfully absorbed into the matrix of aluminium 6061, as seen by the SEM photos, which confirm this. To confirm the presence of the elements in the created composites, XRD analysis is utilised.

The results of the experiment demonstrate that the inclusion of TiO<sub>2</sub> increases the hardness of the generated composites due to Hall Petch strengthening. The hardness test is conducted using a Brinell hardness tester.

The wear properties of the aluminium AA 6061-TiO<sub>2</sub>-Redmud composites are described. Experimental findings and statistical confirmations show that adding reinforcements, particularly red mud and TiO<sub>2</sub>, lowers the specific wear rate (SWR) and coefficient of friction (COF). The experimental findings are confirmed by the statistical analysis of the wear

results, and the projected results closely match the experimental values. The difference between the results of the experiment and the expected values is within a +/-10% range.

The SWR for the as-cast specimen for the R1 experimental trial (load of 10 N, sliding distance of 500 m, and disc rotation speed of 200 rpm) is maximum (0.00626 mm<sup>3</sup>/m), while the SWR for the AR2T4 composite specimen with 2 wt.% red mud and 4 wt.% TiO<sub>2</sub> for the R27 experimental trial is minimum (0.00128 mm<sup>3</sup>/m) (load of 30 N, sliding distance of 2500 m, and disc rotation speed of 600 rpm).

The COF is highest for the As Cast composite specimen (0.411) for the R9 experimental trial, which involves a load of 30 N, a sliding distance of 2500 m, and a disc rotation speed of 600 rpm, while the COF is lowest for the AR2T4 composite specimen for the R19 experimental trial, which involves a load of 10 N, a sliding distance of 500 m, and a disc rotation speed of 200 rpm. In addition, the red mud and TiO<sub>2</sub> reinforcements cause thick friction films to develop, which lowers the wear rate of the composite specimens as seen in the SEM photos of the wear track.

From the results of the current study, it is clear that adding a hybrid reinforcement made of red mud and TiO<sub>2</sub> up to a specific threshold limit enhances the tribological properties of the composites.

#### **Data Availability:**

Data will be made available based on the request to the corresponding author.

#### **V. REFERENCES**

- [1] Kempaiah, U.N.; Santhosh, N.; Kumar, D.H.; Chelgeri, A.H.; Vishnu, P.; Raorane, S. Characterization of High performance Al 5083/SiC/Fly Ash hybrid metal matrix composite for advanced Aerospace Applications. *Int. J. Adv. Innov. Res.* 2015, 3, 334-341.
- [2] Gowda, A.C.; Girish, D.P.; Santhosh, N.; Kumar, A. Study of Wear Characteristics of Aluminium/B<sub>4</sub>C/CNT Hybrid Composites under the Influence of Controlled Factors. *Nano Trends A J. Nanotechnol. Its Appl.* 2016, 18, 21-32.
- [3] Santhosh, N.; Kempaiah, U.N.; Venkateswaran, S. Vibration Mechanics of Hybrid Al 5083/SiC/Fly Ash Composite Plates for its Use in Dynamic Structures. *J. Exp. Appl. Mech.* 2017, 8, 11-18.
- [4] Santhosh, N.; Kempaiah, U.N.; Sajjan, G.; Gowda, A.C. Fatigue Behaviour of Silicon Carbide and Fly Ash Dispersion Strengthened High Performance Hybrid Al 5083 Metal Matrix Composites. *J. Miner. Mater. Charact. Eng.* 2017, 5, 274-287.
- [5] Santhosh, N.; Kempaiah, U.N. Vibration Characterization of SiC and Fly Ash Dispersion Strengthened Aluminium 5083 Composites. *J. Aerosp. Eng. Technol. (JoAET)* 2017, 7, 61-72.
- [6] Santhosh, N.; Kempaiah, U.N.; Bhanupratap, R. Critically Damped Composite plates for Structural applications in Smart Cities. In *Proceedings of the International Conference on Development of Smart Cities, Interface, Governance & Technology*, Dr Ambedkar Institute of Technology, Bangalore, Karnataka, India, 9-10 September 2016.
- [7] Sadashiva, M.; Shivanand, H.K.; Rajesh, M.; Santhosh, N. Corrosion Behavior of Friction Stir Welded Al 6061 Hybrid Metal Matrix Composite Plates. In *Proceedings of the International Conference on Advances in Mechanical Engineering Sciences (ICAMES-17)*, PESCE, Mandya, Karnataka, India, 21-22 April 2017.
- [8] Santhosh, N.; Kempaiah, U.N.; Gowda, A.C.; Rao, S.; Hebbar, G. Evaluation of Corrosion Mechanics of Silicon Carbide and Fly Ash Reinforced Hybrid Aluminium Metal Matrix Composites. In *Proceedings of the International Conference on Emerging Research in Civil, Aeronautical & Mechanical Engineering, ERCAM 2017*, Nitte Meenakshi Institute of Technology, Bengaluru, India, 21 July 2017; pp. 214-218.
- [9] Ramesha, K.; Sudershanan, P.D.; Santhosh, N. Mechanical and Thermal characterization of Friction Stir weld joints of Al-Mg alloy. In *Proceedings of the International Conference on Emerging Trends in Mechanical Engineering (ETME)*, Mandya, India, 27-29 December 2017.
- [10] Santhosh, N.; Kempaiah, U.N. Effect of heat treatment and reinforcements on mechanical properties of aerospace grade Aluminium composites at elevated temperatures. In *Proceedings of the 2nd International Conference on Recent Research Emerging Trends in Mechanical & Civil Engineering, (ICRRETMCE-2018)*, REVA University, Bengaluru, Karnataka, India, 13-14 July 2018.
- [11] Santhosh, N.; Kempaiah, U.N. Effect of silicon carbide and fly ash on characteristics of Aluminium matrix composites for improved dynamic performance. In *Proceedings of the Advanced Ceramics and Nano materials for Sustainable Development (ACeND-2018)*, CHRIST, Bangalore, Karnataka, India, 19-21 September 2018.
- [12] Santhosh, N.; Kempaiah, U.N.; Sunil, G.S. Novel Aluminium-SiC-Fly Ash Hybrid Metal Matrix Composites: Synthesis and Properties. *J. Aerosp. Eng. Technol.* 2017, 7, 26-33.
- [13] Santhosh, N.; Kempaiah, U.N. Influence of Ceramic Particulate Reinforcements on Fly Ash Dispersion Strengthened Composites for Aircraft Structures. *J. Aerosp. Eng. Technol. (JoAET)* 2017, 7, 38-45.
- [14] Trzepieciński, T.; Najm, S.M.; Sbayti, M.; Belhadjalah, H.; Szpunar, M.; Lemu, H.G. New Advances and Future Possibilities in Forming Technology of Hybrid Metal-Polymer Composites Used in Aerospace Applications. *J. Compos. Sci.* 2021, 5, 217.
- [15] Santhosh, N.; Khan, G.M.; Dubey, A.; Patel, S.; Phookan, A. Fabrication and Characterization of Tensile Properties of Aluminium 5083/Silicon Carbide/Fly Ash Composites for Advanced Engineering Applications. *J. Polym. Compos.* 2018, 6, 6-9.
- [16] F. Rana, D.M. Stefanescu, Friction properties of Al-1.5 Pet Mg/SiC particulate metal-matrix composites, *Metallurgical and Materials Transactions A* 20 (1989) 1564-1566.
- [17] K.S. Al Rubaie, H.N. Yoshimura, D.B. Mello, Two-body abrasive wear of Al-SiC composites, *Wear* 233-235 (1999) 444-454.

- [18] Y. Sahin, Optimization of testing parameters on the wear behaviour of metal matrix composites based on the Taguchi method, *Materials Science and Engineering A* 408 (2005) 1–8.
- [19] 50. Mokashi, I.; Afzal, A.; Khan, S.A.; Abdullah, N.A.; Bin Azami, M.H.; Jilte, R.; Samuel, O.D. Nusselt number analysis from a battery pack cooled by different fluids and multiple back-propagation modelling using feed-forward networks. *Int. J. Therm. Sci.* 2020, 161, 106738.
- [20] Santhosh N, Manjunath N, Mahesh H R, Potentiodynamic Corrosion Characterization of Hybrid Aluminium Composites for Advanced Engineering Applications, *International Journal of Engineering and Advanced Technology*, 9(3), 1434-1437, 2020.
- [21] Akhtar, M.; Sathish, T.; Mohanavel, V.; Afzal, A.; Arul, K.; Ravichandran, M.; Rahim, I.; Alhady, S.; Bakar, E.; Saleh, B. Optimization of Process Parameters in CNC Turning of Aluminum 7075 Alloy Using L27 Array-Based Taguchi Method. *Materials* 2021, 14, 4470.
- [22] M. Sadashiva, N.M. Siddeshkumar, J. Monica, M.R. Srinivasa, N. Santhosh, S. Praveenkumar, Hardness and Impact Strength Characteristics of Al based Hybrid Composite FSW Joints, 2022. *Int. J. Vehicle Structures & Systems*, 14(1), 13-17, <https://doi.org/10.4273/ijvss.14.1.04> (SCOPUS). Print (ISSN 0975-3060) and Online (ISSN 0975-3540)
- [23] Meignanamoorthy, M.; Ravichandran, M.; Mohanavel, V.; Afzal, A.; Sathish, T.; Alamri, S.; Khan, S.; Saleel, C. Microstructure, Mechanical Properties, and Corrosion Behavior of Boron Carbide Reinforced Aluminum Alloy (Al-Fe-Si-Zn-Cu) Matrix Composites Produced via Powder Metallurgy Route. *Materials* 2021, 14, 4315.
- [24] K. Ramesha, N. Santhosh, K. Kiran, N. Manjunath, H. Naresh, Effect of the Process Parameters on Machining of GFRP Composites for Different Conditions of Abrasive Water Suspension Jet Machining, 9(94):1-11,2019. [Web of Science and Scopus]
- [25] Sathish, T.; Kaladgi, A.; Mohanavel, V.; Arul, K.; Afzal, A.; Aabid, A.; Baig, M.; Saleh, B. Experimental Investigation of the Friction Stir Weldability of AA8006 with Zirconia Particle Reinforcement and Optimized Process Parameters. *Materials* 2021, 14, 2782.
- [26] BA Praveena, N Santhosh, DP Archana, Abdulrajak Buradi, E Raj, C Chanakyan, Ashraf Elfasakhany, Dadapeer Basheer, Influence of Nanoclay Filler Material on the Tensile, Flexural, Impact, and Morphological Characteristics of Jute/E-Glass Fiber-Reinforced Polyester-Based Hybrid Composites: Experimental, Modeling, and Optimization Study, *Journal of Nanomaterials* Vol. 2022, Article ID 1653449, 17 pages <https://doi.org/10.1155/2022/1653449>.
- [27] Nagaraja, S.; Kodandappa, R.; Ansari, K.; Kurunian, M.S.; Afzal, A.; Kaladgi, A.R.; Aslfattahi, N.; Saleel, C.A.; Gowda, A.C.; Bindiganavile Anand, P. Influence of Heat Treatment and Reinforcements on Tensile Characteristics of Aluminium AA 5083/Silicon Carbide/Fly Ash Composites. *Materials* 2021, 14, 5261. <https://doi.org/10.3390/ma14185261>.
- [28] G Ravichandran, G Rathnakar, N Santhosh, R Suresh, Wear Characterization of HNT filled Glass-Epoxy Composites using Taguchi's Design of Experiments and Study of Wear Morphology, *Composites Theory and Practice*, 2020, 20(2), 85-91.
- [29] G Ravichandran, G Rathnakar, N Santhosh, R Thejaraju, Antiwear Performance Evaluation of Halloysite Nanotube (HNT) Filled Polymer Nanocomposites, *International Journal of Engineering and Advanced Technology*, 2019, 9(1), 3314-3321.
- [30] Srinivasa M. R., Y. S. Rammohan, Sadashiva M., Santhosh N, Effect of Shock Waves on the Hardness of Graphene Reinforced Aluminium Composites, *Journal of Polymer & Composites*, 8(1), 32-38, 2020.
- [31] Ramesha K, Sudersanan, P D, Santhosh N, Sasidhar Jangam. 2021. "Corrosion Characterization of Friction Stir Weld Joints of Dissimilar Aluminum Alloys.", *EAI/Springer Innovations in Communication and Computing*, <https://doi.org/10.4108/eai.16-5-2020.2304097>
- [32] Ramesha K, Sudersanan, P D, Santhosh N, Sasidhar Jangam. Sustainable Processing of Dissimilar Aluminium Alloy Joints by Friction Stir Welding, *IOP Conf. Series: Materials Science and Engineering* 1132 (2021) 012029, IOP Publishing, <https://iopscience.iop.org/article/10.1088/1757-899X/1132/1/012029>.
- [33] Ramesha K, Sudersanan, P D, Santhosh N, Sasidhar Jangam, (2021). Design and optimization of the process parameters for friction stir welding of dissimilar aluminium alloys. *Engineering and Applied Science Research*, 48(3), 257-267. <https://ph01.tci-thaijo.org/index.php/easr/article/view/241021>.
- [34] K. Ramesha, P. D. Sudersanan, Prem Kumar Mahto, Shaikh Mohammed Ismail, Ashwin C. Gowda, N. Santhosh and V. Umesh, Influence of heat treatment on the tensile and hardness characteristics of friction stir weld joints of dissimilar aluminium alloys, *AIP Conference Proceedings* Vol. 2421, Issue -1, Pages 030001 (2022); <https://doi.org/10.1063/5.0076766> (SCOPUS). ISSN: 0094-243X (print) 1551-7616 (web)
- [35] K. Ramesha, P.D. Sudersanan, A.C. Gowda, N. Santhosh, S. Jangam, N. Manjunath, Friction Stir Welding of Dissimilar Aluminium Alloys for Vehicle Structures, *Int. J. Vehicle Structures & Systems*, Vol. 14 No. 1 (2022), 5 – 9, <https://doi.org/10.4273/ijvss.14.1.02> (SCOPUS). Print (ISSN 0975-3060) and Online (ISSN 0975-3540)
- [36] N. Santhosh , B. A. Praveena , H. V. Srikanth , Santosh Angadi , Amaresh Gunge , M. Rudra Naik , G. Shankar , K. Ramesha , G. Ravichandran, Experimental Investigations on Static, Dynamic, and Morphological Characteristics of Bamboo Fiber-Reinforced Polyester Composites, *Hindawi, International Journal of Polymer Science* Volume 2022, Article ID 1916877, 11 pages <https://doi.org/10.1155/2022/1916877>.
- [37] N Santhosh , B A Praveena, A Chandrashekar, V Mohanavel, S Raghavendra, Dadapeer Basheer, Wear behaviour of aluminium alloy 5083/SiC/fly ash inoculants based functional composites- optimization studies, *Mater. Res. Express* 9 (2022) 076513, <https://doi.org/10.1088/2053-1591/ac8229>.
- [38] Nagaraja, S; Nagegowda, K.U.; Kumar V, A.; Alamri, S.; Afzal, A.; Thakur, D.; Kaladgi, A.R.; Panchal, S.; Saleel C, A. Influence of the Fly Ash Material Inoculants on the Tensile and Impact Characteristics of the Aluminum AA 5083/7.5SiC Composites. *Materials* 2021, 14, 2452. <https://doi.org/10.3390/ma14092452>.
- [39] Bharath, V.; Auradi, V.; Kumar, G.B.V.; Nagaral, M.; Chavali, M.; Helal, M.; Sami, R.; Aljuraide, N.; Hu, J.W.; Galal, A.M. Microstructural Evolution, Tensile Failure, Fatigue Behavior and Wear Properties of Al<sub>2</sub>O<sub>3</sub> Reinforced Al<sub>2</sub>O<sub>14</sub> Alloy T6 Heat Treated Metal Composites. *Materials* 2022, 15, 4244. <https://doi.org/10.3390/ma15124244>.